EXPERIMENTAL ACTIVE CONTROL OF A TYPICAL SECTION AIRFOIL USING A TRAILING EDGE FLAP

Jeffrey S. Vipperman [¤]   Robert L. Clark [y]   Mark Conner [z]

Earl H. Dowell [x]

Department of Mechanical Engineering and Materials Science

Box 90300

Duke University, Durham, NC 27708-0300

June 26, 1997

Abstract

This paper presents an experimental implementation of an active control system used to suppress flutter in a typical section airfoil. The H_2 optimal control system design is based upon experimental system identifications of the transfer functions between three measured system variables: pitch, plunge, and flap position and a single control signal which commands the flap of the airfoil. Closed-loop response of the airfoil demonstrated gust-alleviation below the open-loop flutter-boundary. In addition, the flutter boundary was extended by 12.4% through the application of active control. Cursory robustness tests demonstrate stable control for variations in flow-speed of $\S 10\%$.

[¤]Graduate Research Assistant, Student Member AIAA
[y]Assistant Professor, Member AIAA
[z]Graduate Research Assistant
[x]Dean of Engineering, J. B. Jones Professor of Mechanical Engineering and Materials Science, Fellow AIAA

Introduction

Active control of articulated aerodynamic control surfaces has been a topic of interest for many years. Various control strategies including classical, modern (LQR/LQG) and robust (H_∞) have been applied to structures ranging in complexity from typical sections,[1] to cantilevered wings.[2-4] The objective has typically been two-fold: provide gust alleviation for ride quality and extend the flutter boundary for performance. While a significant effort has been devoted to analytical studies,[5-10] there are fewer experimental implementations of closed-loop controllers.[1-4,11] At NASA Langley Research Center, the Benchmark Active Controls Testbed (BACT)[12] has been used to generate extensive test data and dynamic models[13] dedicated to the study of flutter suppression controllers. The physics associated with the control problem are well described by Edwards et al.,[6] Karpel,[14] and Lazarus et al.[15]

The objective of the proposed effort was to investigate experimentally, the closed-loop performance of a three degree-of-freedom (dof) typical section using a trailing edge flap as the control input and measures of pitch, plunge and flap actuator position as sensor variables. While analytical models of the system have been developed,[8,16,17] an experimental system identification was performed at each dynamic pressure (flow speed) for which the controller was designed. An H_2 controller was designed which minimized the power associated with pitch, plunge, and flap position upon exciting each state of the measured system with stochastic noise sources. The objective was to create a compensator which would provide gust alleviation at flow speeds well below the flutter boundary and extend the flutter boundary at the upper limit. Based upon the experimental system identification, both predicted and measured performance are compared.

Since the poles and zeros of the dynamic system vary as a function of dynamic pressure (flow speed for wind-tunnel experiments), the compensators demonstrated limited robustness to variation in flow speed. In general, the controllers provided stability at flow speeds $\pm$ 10% of that for which they were designed. Thus, it is not unreasonable to expect a limitation in the extension of the flutter boundary beyond 10%. However, once the flutter boundary is extended, one can identify the system response at the higher flow speed and use this data to design a

controller which will stabilize the system at yet higher °ow speeds. Since gain scheduling is required, one could identify the closed-loop system on-line and use this data to determine the compensator necessary for operation at higher dynamic pressures.

Control Strategy

The control system was synthesized by casting the aeroelastic control problem into a two-port con¯guration using linear quadratic Gaussian (LQG)-style weighting parameters as shown in Figure 1. From Figure 1, the generalized plant, $\mathbf{G}(\mathbf{s})$ consists of the Aeroelastic model, $\mathbf{fA; B; C; Dg}$ as well as subsystems which determine the frequency-domain shape of the process noise, sensor noise, control penalty and performance penalty, which were chosen to be \°at" or all-pass. Also from Figure 1, $\mathbf{w}(\mathbf{t})$ is a vector of disturbance inputs composed of process noise, »(t), and sensor noise, μ(t), which were assumed to be uniform random processes. For simplicity, each state of the aeroelastic model was excited uniformly by the process noise, »(t): The output, $\mathbf{z}(\mathbf{t})$, is an error or performance vector which allows the performance objective (minimize pitch, plunge and °ap) to be traded o® with control e®ort. Finally, the vector $\mathbf{y}(\mathbf{t})$ is the set of measured variables (pitch, plunge and actuator position) which are fed back to form the scalar control signal, $\mathbf{u}(t)$ that commands the °ap.

Note that the variables measured in vector $\mathbf{y}(\mathbf{t})$ that are fed back to form the control signal are also the plant variables that partially comprise the performance penalty, $\mathbf{z}(\mathbf{t})$; and are thus minimized by the controller. An experimental system identi¯cation is performed to determine the Aeroelastic model, $\mathbf{fA; B; C; Dg}$: A total of 27 states were used in the curve-¯t which allowed the less-signi¯cant dynamics to be modelled as well.

The objective is to ¯nd the controller which minimizes the $\mathbf{k}\,T_{\mathbf{wz}}\,\mathbf{k}_2$ of the closed-loop transfer function from $\mathbf{w}$ to $\mathbf{z}$: $T_{\mathbf{wz}}$, (Doyle, et al., 1989), where

$$\mathbf{k}\,T_{\mathbf{wz}}\,\mathbf{k}_2 \quad := \quad \left[\frac{1}{2\pi} \int_{-1}^{1} \text{trace}\,[T_{\mathbf{wz}}(j\omega)^{\ast}T_{\mathbf{wz}}(j\omega)]\,d\omega \right]^{1=2} \tag{1}$$

where $\mathbf{k}\,\mathbf{\dot{c}}\,\mathbf{k}_2$ is the 2-norm, $T_{\mathbf{wz}}$ is the transfer function from $\mathbf{w}$ to $\mathbf{z}$ (disturbance input to performance output), $\ast$ denotes the complex conjugate operator, $j = \sqrt{-1}$, and ! is the natural

3

circular frequency. A block diagram of the quadruple describing the system is illustrated in Figure 2. The input signals represented by the vector, **w**, contain both sensor noise and the disturbance, while **z** is vector of performance output signals which for the given system includes both the error signals and the control effort signal. The control input to the moving coil transducer is represented by **u**, and the measured signals are represented by **y**. If a frequency weighted cost functional is desired, one can readily replace the static or all-pass filters included within this model with dynamic filters in formulating the augmented system. Thus, for the chosen formulation, the LQG problem is embedded within the augmented system. The formal solution for the unique optimal controller can be found in the reference by Doyle et al.[18]

System Description

Wing Model

The experimental model is shown in Figure 3. The NACA 0012 rectangular wing model includes two parts, a main wing with a 19 cm chord and 52 cm span and a flap with a 6.35 cm chord and 52 cm span, which is mounted at the trailing edge of the main wing using two pairs of micro-bearings with pins allowing the flap to have a rotational degree-of-freedom relative to the main wing. The main wing is constructed from an aluminum alloy circular spar beam with a diameter of 2.54 cm and a wall thickness of 0.32 cm. The beam runs through 14 pieces of NACA 0012 aluminum airfoil plate and serves as the pitch axis, located at the quarter-chord location from the leading edge. A 0.254 mm thick aluminum sheet covers the entire chord and span, providing the aerodynamic contour of the wing. The flap is constructed in a similar manner with an aluminum alloy tube spar beam (1.27 cm diameter and 0.16 cm wall thickness) passed through the leading edge of 14 pieces of NACA 0012 wood airfoil plate. The flap is also covered with the same type of aluminum sheet.

The model dimensions were chosen to try to maintain a two-dimensional flowfield by minimizing the end effects and (thickness to wall-separation). Inertial and stiffness parameters were chosen to yield a flutter speed that was well below the maximum attainable speed for the wind

4

tunnel.

Support Structure

As seen in Figure 3, the model is mounted vertically in the wind tunnel. The support mechanisms for the model are mounted outside of the wind tunnel, at the top and bottom. Each support mechanism consists of a guided cantilever beam[19] made of two steel leaf springs which are 20.32 cm long, 2.86 cm wide and 0.102 cm thick. Figure 4 shows the upper support mechanism which is identical to its lower counterpart. The distance between the two leaf springs which make up each guided cantilever beam is 15.24 cm. A support block joins the free ends of the two leaf springs and these upper and lower support blocks move with the model along the plunge degree-of-freedom. The pitch axis of the main wing is mounted to the upper and lower support blocks through a pair of precision bearings which have a small amount of dry friction in the ball. At the upper bracket, there is a spring wire which is press-¯t through the center of the shaft that forms the pitch axis and simply-supported at each end to form the pitch sti®ness. Supports at each end of the spring wire can be moved in or out to increase or decrease, respectively, the sti®ness of the pitch axis. The sti®ness and inertial properties of the airfoil before the addition of the control actuator assembly can be found in the literature.[16]

Control Actuator Assembly

A schematic of the experimental control assembly is shown in Figure 5. A BEI linear actuator, LA13-12-000A, serves as the means of applying the required control force to the experimental model. The ¯eld assembly has a diameter of 3.16 cm, and the coil assembly has a diameter of 2.6 cm. The actuator has a free stroke of §0:3175 cm, with a total length (¯eld and coil assemblies) of 2.86 cm at mid-stroke. The system can apply a peak force of 15.57 N and a blocked force of 7.12 N. The ¯eld assembly is held stationary in a support block that is mounted to a base plate used to support all of the control system hardware. Two precision linear bearings are mounted on the base plate and support a mating precision shaft that is threaded into the center of the coil assembly. The bearings allow the coil assembly to move in and out of the ¯eld

assembly while maintaining the speci¯ed clearance between the two. The base plate containing all of the control system hardware is mounted at one end of the wing model, as shown in Figure 6. The total mass of the actuator assembly is 0.419 kg.

The position of the coil assembly is measured using a Lucas Schaevitz 250 MHR linear variable displacement transducer (LVDT), shown in Figure 5. The core of the LVDT is attached to the shaft, and the body of the LVDT is mounted in a support block. In addition to the actuator position, two other displacement measurements are also fed back for the system control. The pitch angle of the main wing is measured by a rotational variable displacement transducer (RVDT) which is ¯xed at the upper end of the pitch axis. The plunge displacement is measured using another RVDT which remains stationary relative to the motion of the upper support block. Figure 4 denotes the two RVDTs used to measure pitch and plunge. The three measurement signals are independent of each other.

Since the linear motion of the actuator is being converted into the rotational motion of the °ap, a small amount of °exibility in the connection is required. The actuator shaft and the shaft extending from the control surface are perpendicular to each other and are joined by a thin, rectangular piece of fairly sti® spring steel, which keeps the actuator shaft from binding as it moves through its entire range of travel. A moment arm that is 2.0 cm long is achieved by the °exible linkage. The entire control assembly is mounted to the lower end of the wing-aileron. A cutout must be made in the °oor of the tunnel to allow the actuator assembly to extend beyond the main wind tunnel test section. The cutout is large enough for the control assembly and allows for a reasonable range of motion. Since the control system is mounted to the main wing, the entire assembly will pitch and plunge with the airfoil. Flap actuator position was fed back to the control system in lieu of °ap angle since slightly better coherence with the command signal was measured. The actuator/aileron connector shim added a damped resonance at 125 Hz, which is much higher than the dynamics of the typical section. Measured frequency response functions (FRFs) between °ap angle and control input and °ap actuator position and control input are identical between 0-20 Hz, which encompasses the dynamics of the typical section.

Measured airfoil resonances at 6.34, 11.0, and 12.4 Hz (in the absence of flow) are associated with plunge, pitch, and flap, degrees-of-freedom respectively.

Wind Tunnel

All tests of the two-dimensional wing model were performed in the Duke University low speed wind tunnel. The wind tunnel is a closed circuit tunnel with a test section of 0.70 m x 0.51 m and a length of 1.22 m. The maximum attainable air speed is 89 m/s. The stagnation temperature of the airstream is held constant over the range 15º C to 38º C by means of an external air exchange system and tunnel stagnation pressure equals atmospheric pressure at the low Reynolds number operating conditions. For the present test, the Reynolds number based upon model chord is 0.52×10^6.

Controller Implementation

The control designs were implemented in discrete time on a TMS320C31-based digital signal processor (DSP) board manufactured by Spectrum Signal Processing, Inc. A Spectrum Signal Processing 16-input, 8-output Multi-I/O board was used to sample the continuous time signals as well as reconstruct digital signals back into analog. Each control design was discretized using a Tustin transform.[20] The controller parameters were downloaded to the DSP using a Pentium^{TM}-based computer, which hosted the DSP board.

The sampling rate was set to 2 kHz for all experiments, which provided ample bandwidth for the control problem, which mainly focused on dynamics in a 0-20 Hz frequency band. Most control systems had 25 states after a very modest model reduction, but the final control system which was based on a system identification performed on a closed-loop system above the original flutter boundary contained 61 states.

System Identification

In order to design a controller for experimental implementation, a system identification of the wind tunnel model has been performed. A Tektronix 2630 Spectrum Analyzer was used

to calculate the frequency response functions (FRFs) and coherences between a random input to the actuator and the resulting responses from each of the three outputs: pitch, plunge and actuator displacements. The random input signal generated by the Tektronix analyzer was ampli¯ed by a Hewlett-Packard 6825A Bipolar Power Supply/Ampli¯er and then sent to the terminals of the linear actuator.

Frequency response function (FRF) data were recorded for the linear system for freestream conditions ranging from no freestream velocity to speeds near the °utter boundary. SmartID[21] software was then used to do a multi-variable system identi¯cation and provide a state-space model of the aeroelastic system. Using twenty-seven states to model the dynamics of the system provided adequate ¯ts for the magnitude and phase for all three transfer functions at each of the °ow conditions. The measured magnitude and phase along with the approximation from the system identi¯cation is shown in Figure 7 for a representative °ow condition, 18.1 m/s. The approximations, which are shown by the dotted lines, match well with both the magnitude and phase of the experimentally measured FRFs which are shown by the solid lines. Each frequency-domain experimental FRF has the 95% con¯dence bounds plotted in very thin lines. It is di±cult to see the narrow lines that mark the con¯dence bounds in Figure 7 since they are nearly coincident with the bold lines that represent the data. The con¯dence bounds are computed using the estimate of the coherence function between the input and output signals for the FRF, which takes into account many bias errors including input noise, estimation biases, nonlinearities and time-varying properties. The °utter speed for the experimental system without control is approximately 18.6 m/s.

It should be noted that the coherence between the random input to the actuator and the pitch and plunge motion of the typical section model increases as the freestream velocity increases. With the increase in airspeed comes an increase in the °uid-structure coupling that characterizes aeroelastic systems. The increased coupling allows for a more accurate system identi¯cation and more controllability, which ameliorates control system design.

Results

Controllers were designed based upon each of the system identi¯cations discussed previously. For the sake of brevity, only two of the pre-°utter cases will be discussed here. Also, only the magnitude portion of the frequency responses is shown, although the phase data also showed very good correlation.

\Low" Freestream Velocity

Figure 8 (a) - (c) shows the predicted open and closed loop frequency responses for pitch, plunge and actuator displacements, respectively, for a controller designed for an operating °ow speed of 12.5 m/s. The \predicted" responses are obtained by coupling the control designs with the state-space aeroelastic models obtained from the system identi¯cation process. The experimental frequency responses are shown in parts (d) - (f), including the 95% con¯dence bounds in very thin lines, which again are nearly coincident with the data. The predicted frequencies for the primary and secondary peaks are slightly higher than those of the actual system, though they match well in magnitude. The closed loop responses are very similar in nature, showing a signi¯cant decrease in the magnitude of the primary peak along with an increase in magnitude at the secondary peak. The numerical model did predict a reduction of approximately 20 dB at the primary peak, while the actual decrease was closer to 15 dB.

The experimental time domain responses for the pitch and plunge degrees-of-freedom at 12.5 m/s are shown in Figure 9. The model was given an initial displacement in the plunge degree-of-freedom of 3.5 mm and was then released. A signi¯cant increase between the overall damping of the open and closed loop systems is seen in both of the time series. The controlled system response decays in about one-fourth the time of the uncontrolled system. Con¯dence bounds for the time-domain plot are not included since they were characterized in the frequency domain.

\High" Freestream Velocity

The increased accuracy of the system identiˉcation at higher °ow conditions can be seen in Figure 10, showing the frequency response using a controller designed for an operating freestream velocity of 18.1 m/s. While the correlation between the predicted and experimental frequency responses were very good at the lower °ow speed, the predicted and measured open and closed loop curves now lie almost on top of each other. The largest di®erence occurs around 10 Hz, where the numerical model again predicts worse behavior than is seen experimentally. The predicted 20 dB reduction at 4.5 Hz was achieved in the wind tunnel experiment.

The open-loop or uncontrolled time responses seen in Figure 11 show that the overall system damping is very low and the °ow conditions are very near the °utter boundary. The open-loop response continues longer than seven seconds while the closed-loop response decays in less than 1.5 seconds. These results do show great potential for increasing the °utter speed.

Flutter Boundary

The °utter speed for the uncontrolled system is approximately 18.6 m/s. Time series for pitch and plunge just past the uncontrolled °utter boundary are shown in Figure 12. An experimental frequency response was obtained for a freestream velocity of 18.5 m/s, and the controller designed for this °ow condition was used to to successfully increase the °utter boundary by approximately 8%. Figure 13 shows the controlled time response at 20.0 m/s (8.1% above the uncontrolled °utter speed). A closed loop frequency response was obtained at 20.1 m/s and is shown in Figure 14a, with the 95% conˉdence bounds plotted in very thin lines again.

Using the post-°utter closed loop frequency response, a new system identiˉcation was performed to obtain a numerical model of the system operating above the uncontrolled °utter boundary. The size of the numerical model increased from twenty-seven states for the pre-°utter conditions to ˉfty states at 20.1 m/s. A new controller was then designed using the new numerical model in order to try to further increase the °utter boundary. Figure 14b shows the closed loop frequency response for the experimental system at 20.9 m/s, which represents an

overall increase in the original °utter boundary of over 12%. The 95% con¯dence bounds plotted in thin lines in Figure 14b are much larger than those plotted in Figure 14a due to a decrease in the coherence estimates, presumably due to the controller interaction and larger aerodynamic excitation at the higher °ow rate.

O®-Nominal Design Performance

The e®ectiveness of each of the controllers away from their nominal design speed was examined numerically and experimentally. Figure 15 shows the open and closed loop pitch responses for °ow conditions at, above, and below the design speed of 16.7 m/s. The predictions at the lower °ow speed of 14.8 m/s show a better correlation with the measured data, as seen in parts (a) and (c). There is a di®erence in magnitudes at very low frequencies. The same trends are seen between the numerical and experimental data for the higher °ow speed of 18.1 m/s, however, there is a noticeable di®erence in the secondary peak. In this case, the actual response is more favorable than that predicted.

Conclusions

Active control of a typical section airfoil using a trailing edge °ap as the control input and measures of pitch, plunge and °ap actuator position as sensor variables was investigated. An experimental system identi¯cation was performed at each dynamic pressure (°ow speed for wind-tunnel experiments), and an H_2 controller was designed for each °ow condition to minimize the RMS power associated with pitch, plunge, and °ap position due to stochastic disturbance sources applied across each aeroelastic state of the system. The resulting compensator provided gust alleviation at °ow speeds well below the °utter boundary and extended the °utter boundary at the upper limit by 12.4%. The predicted and measured closed-loop performance compared well over all °ow conditions, and the resulting compensators designed for a speci¯c °ow condition were observed to provide stable closed-loop performance at °ow speeds varying between § 10% of the nominal.

Results from this work also demonstrate that once the °utter boundary is extended through

the implementation of an active control system, a system identi¯cation of the closed-loop system can be obtained to design a controller which further extends the °utter boundary for higher °ow speeds. If the controller were designed on-line, then one could identify the plant concurrently while implementing control to meet the demands of variation in dynamic pressure.

Future work will address the e®ects of free-play nonlinearities between the °ap actuator and the °ap. In addition, methods of producing a robust control system for all operating conditions (dynamic pressures) using gain-scheduling or structured uncertainty methods will be investigated.

Acknowledgements

References

[1] Mukhopadhyay, V., \Flutter Suppression Control Law Design and Testing for the Active Flexible Wing," Journal of Aircraft, Vol. 32, No. 1, 1995, pp. 45{51.

[2] Lin, C. Y., Crawley, E. F., and Heeg, J., \Open Loop and Preliminary Closed Loop Results of a Strain Actuated Active Aeroelastic Wing," 36th AIAA/ASME/ASCE/AHS/ASC Structures, Structural Dynamics, and Materials Conference, New Orleans, LA, Apr. 10-13 1995, pp. 1904{1914.

[3] Ghiringhelli, G. L., Lanz, M., and Mantegazza, P., \Active Flutter Suppression for a Wing Model," Journal of Aircraft, Vol. 27, No. 4, 1990, pp. 334{341.

[4] Pak, C., Friedmann, P. P., and Livne, E., \Transonic Adaptive Flutter Suppression Using Approximate Unsteady Time Domain Aerodynamics," 32nd AIAA/ASME/ASCE/AHS/ASC Structures, Structural Dynamics, and Materials Conference, 1991, pp. 1832{1854.

[5] Ozbay, H. and Bachmann, G. R., \H_2/H_1 Controller Design for a Two-Dimensional Thin Airfoil Flutter Suppression," Journal of Guidance, Control, and Dynamics, Vol. 17, No. 4, 1994, pp. 722{728.

[6] Edwards, J. W., Breakwell, J. V., and Bryson, A. E., \Active Flutter Control Using Generalized Unsteady Aerodynamic Theory," Journal of Guidance and Control, Vol. 1, No. 1, 1978, pp. 32{40.

[7] Lazarus, K. B., Crawley, E. F., and Lin, C. H., \Fundamental Mechanisms of Aeroelastic Control With Control Surface and Strain Actuation," 32nd AIAA/ASME/ASCE/AHS/ASC Structures, Structural Dynamics, and Materials Conference, 1991, pp. 1817{1831.

[8] Conner, M. D., Tang, D., Dowell, E. H., and Virgin, L. N., \Accurate Numerical Integration of State Space Models for Aeroelastic Systems With Freeplay," AIAA Journal, Accepted for Publication.

[9] Newsom, J. R., \Control Law Synthesis for Active Flutter Suppression Using Optimal Control Theory," Journal of Guidance and Control, Vol. 2, No. 5, 1979, pp. 388{394.

[10] Lin, C. Y. and Crawley, E. F., \Design Considerations for a Strain Actuated Adaptive Wing for Aeroelastic Control," Proceedings, Fourth International Conference on Adaptive Structures, Cologne, Germany, 1993.

[11] Lazarus, K. B. and Crawley, E. F., \Multivariable Active Lifting Surface Control Using Strain Actuation: Analytical and Experimental Results," Third International Conference on Adaptive Structures, 1992, pp. 87{101.

[12] Durham, M. H., Keller, D. F., Bennett, R. M., and Wieseman, C. D., \A Status Report on a Model for Benchmark Active Controls Testing," AIAA-91-1011, 1991.

[13] Waszak, M. R., \Modeling the Benchmark Active Control Technology Wind-Tunnel Model for Application to Flutter Suppression," Proceedings of the AIAA Atmospheric Flight Mechanics Conference, San Diego, CA, July 29-31 1996.

[14] Karpel, M., \Design for Active Flutter Suppression and Gust Alleviation Using State-Space Aeroelastic Modeling," Jornal of Aircraft, Vol. 19, No. 3, 1982, pp. 221{227.

[15] Lazarus, K. B. and Crawley, E. F., \Multivariable High-Authority Control of Plate-Like Active Structures," 33rd AIAA/ASME/ASCE/AHS/ASC Structures, Structural Dynamics and Materials, Dallas, TX, AIAA-92-2529-CP, Apr. 13-15 1992, pp. 931{945.

[16] Conner, M. D., Tang, D., Dowell, E. H., and Virgin, L. N., \Nonlinear Behavior of a Typical Airfoil Section with Control Surface Freeplay: A Numerical and Experimental Study," Journal of Fluids and Structures, Vol. 11, 1997, pp. 89{109.

[17] Conner, M. D., Nonlinear Aeroelasticity of an Airfoil Section With Control Surface Freeplay, Ph.D. thesis, Duke University, Durham, NC 27708, 1996.

[18] Doyle, J. C., Glover, K., Khargonekar, P. P., and Francis, B. A., \State-Space Solutions to Standard H_2/H_1 Control Problems," IEEE Transactions on Automatic Control, Vol. 34, No. 8, 1989, pp. 831{847.

[19] Roark, R. J. and Young, W. C., Roark's Formulas for Stress and strain, McGraw-Hill, New York, 1989.

[20] Oppenheim, A. V. and Schafer, R. W., Digital Signal Processing, Prentice{Hall, Inc., Englewood Cli®s, NJ 07632, 1975.

[21] Active Control eXperts, Inc., 215 First Street, Cambridge MA, 12142, Smart ID System Identi¯cation Software.

List of Figures

Figure 1: Diagram of Two-Port Control Con⁻guration

Augmented System

$$
\begin{array}{c|cc}
A & B_w & B_u \\
\hline
C_z & 0 & D_{zu} \\
C_y & D_{yw} & 0
\end{array}
$$

$w \rightarrow$

$u \rightarrow$

$\rightarrow z$

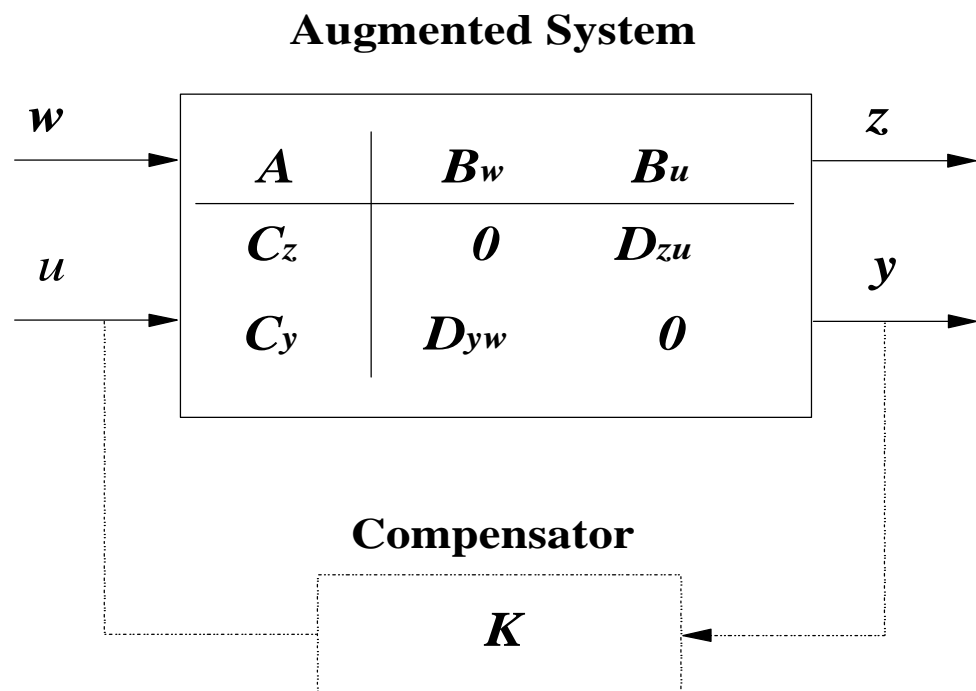$\rightarrow y$

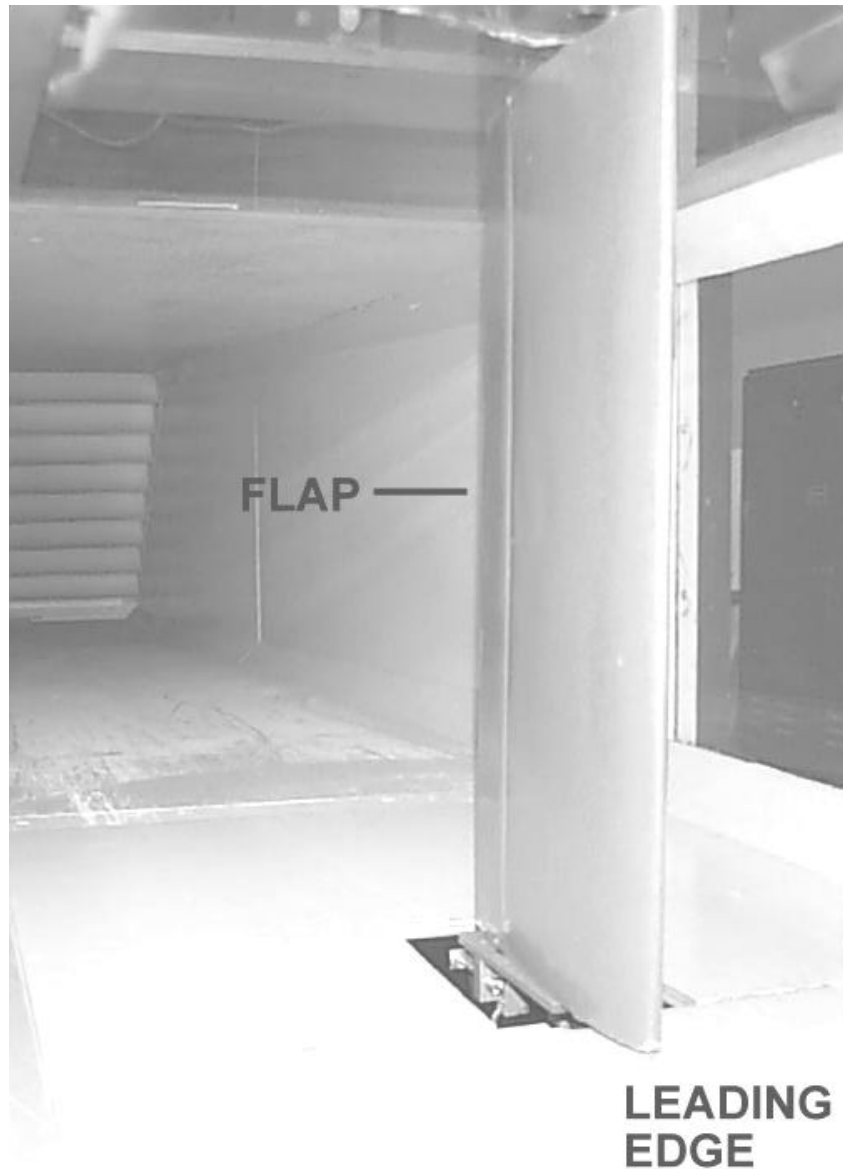**Compensator**

K

Figure 2: Composite Closed-loop System

FLAP ———

LEADING
EDGE

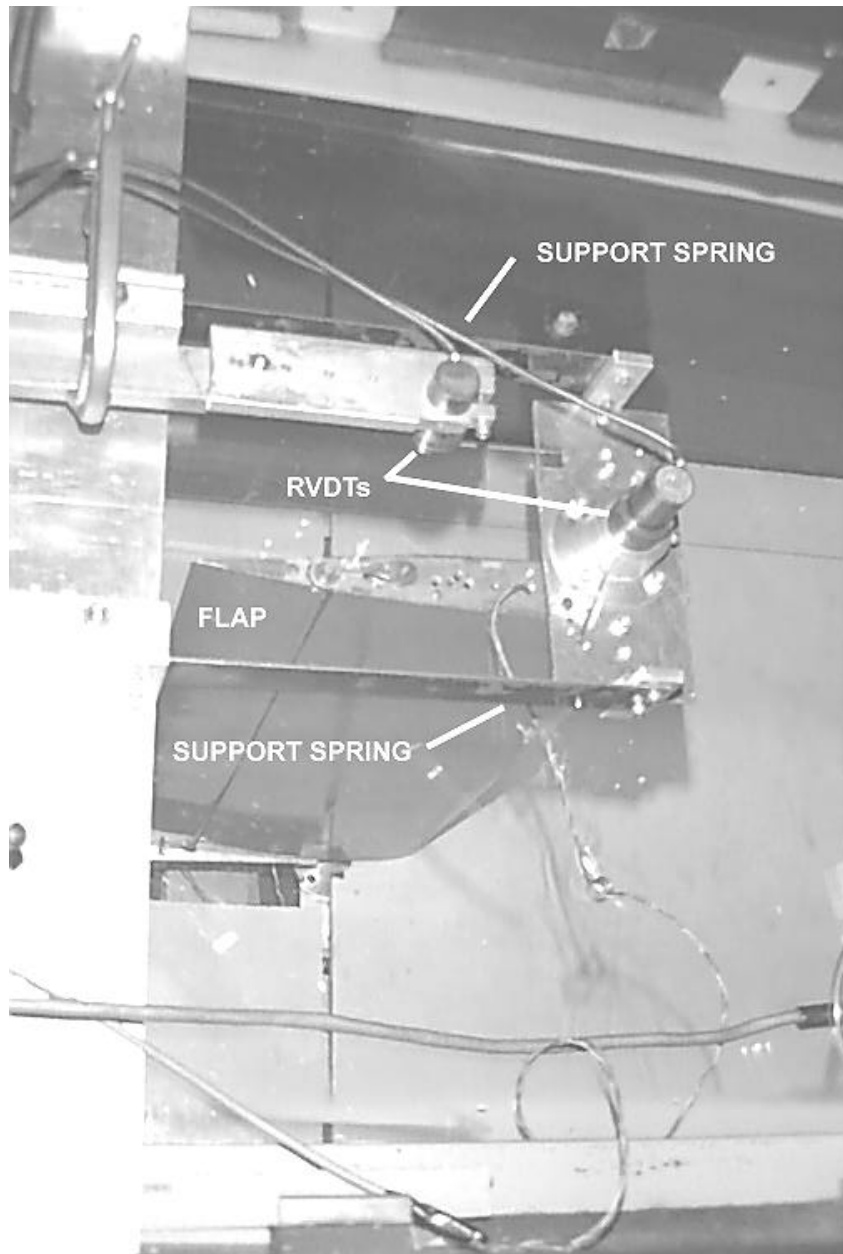Figure 3: Photograph of the Experimental Model, as Mounted in the Duke University Low-Speed Wind Tunnel

Figure 4: Photograph Showing Top Views of the Experimental Model and the Support Structure, as Mounted in the Duke University Low-Speed Wind Tunnel; The Airfoil and Flap Can be Seen Through the Clear, Top Wall of the Wind Tunnel
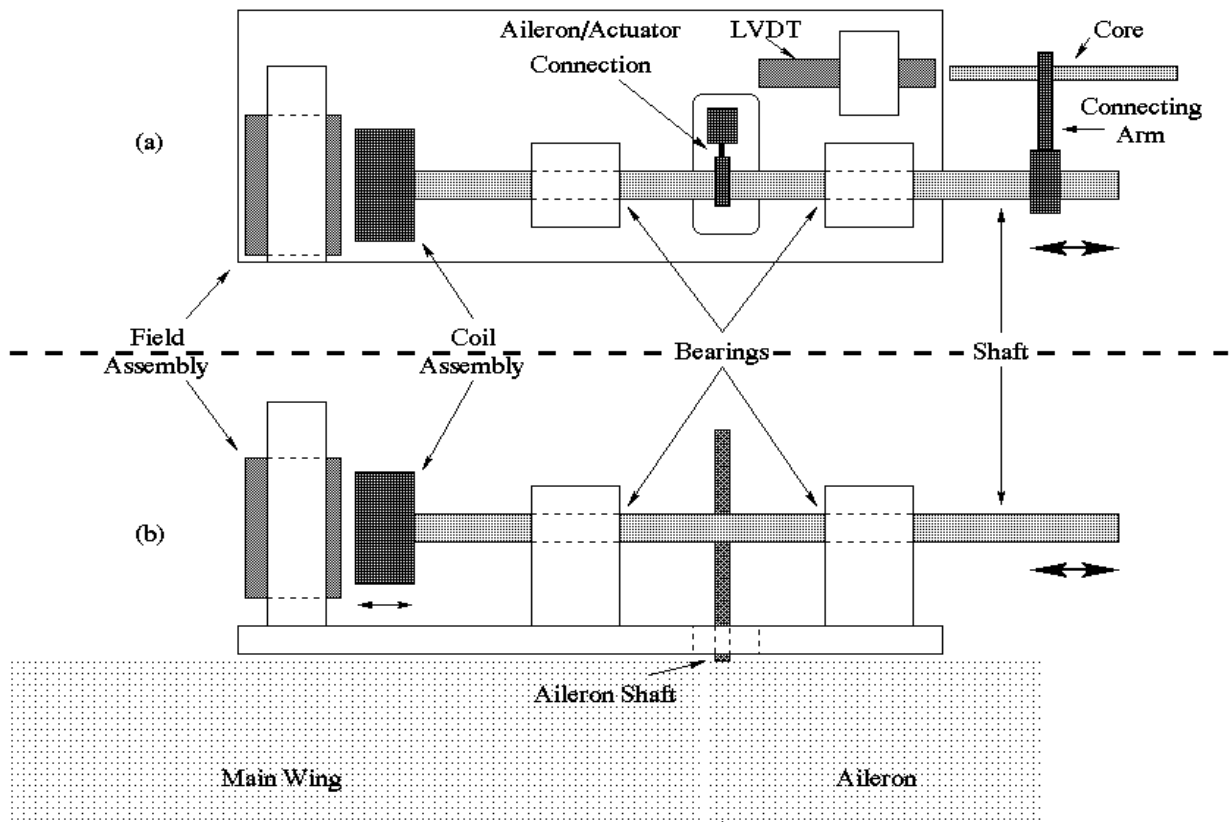
Figure 5: Schematic Diagram of Experimental Control Assembly
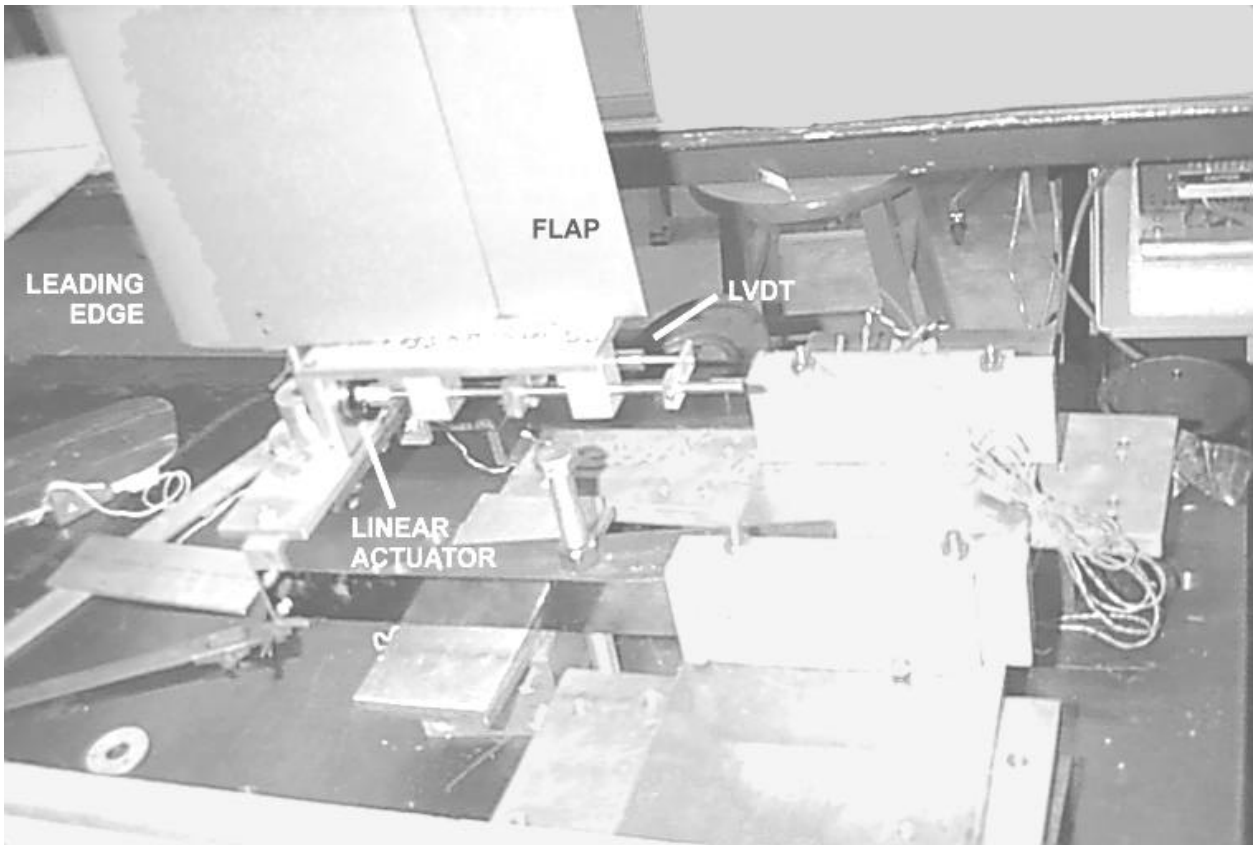
Figure 6: Picture of Control Assembly With Bottom Wall of Wind Tunnel Removed
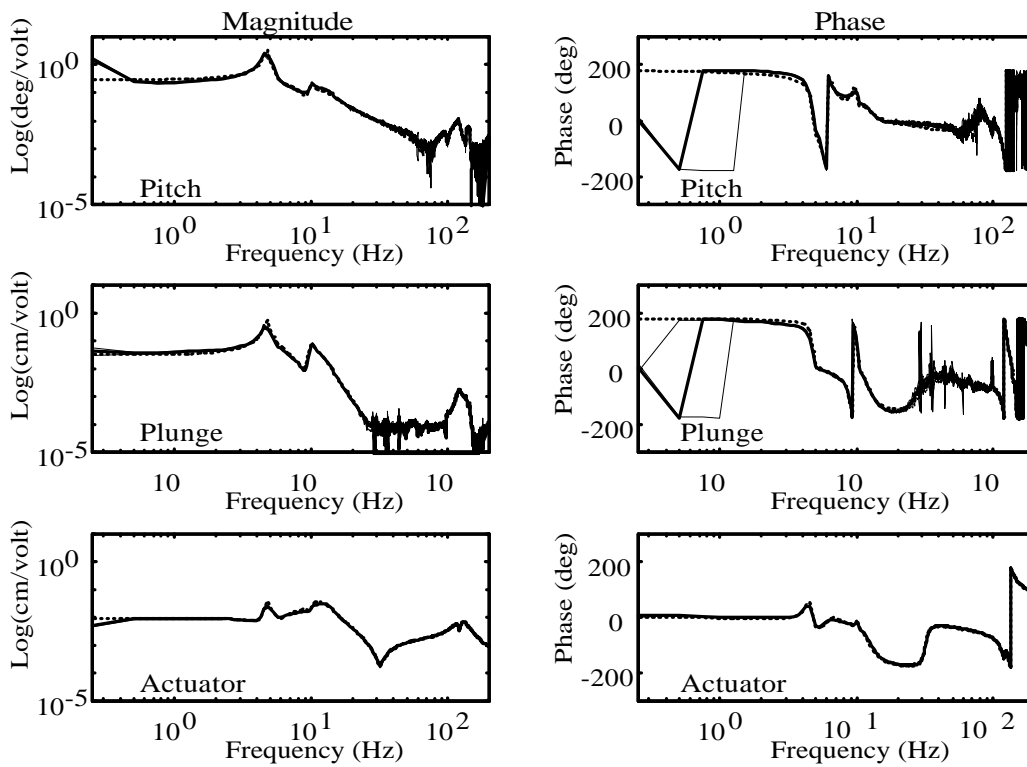
Figure 7: Measured (⎯{) and Modeled (- - -) Frequency Response of the Three Observed System Variables
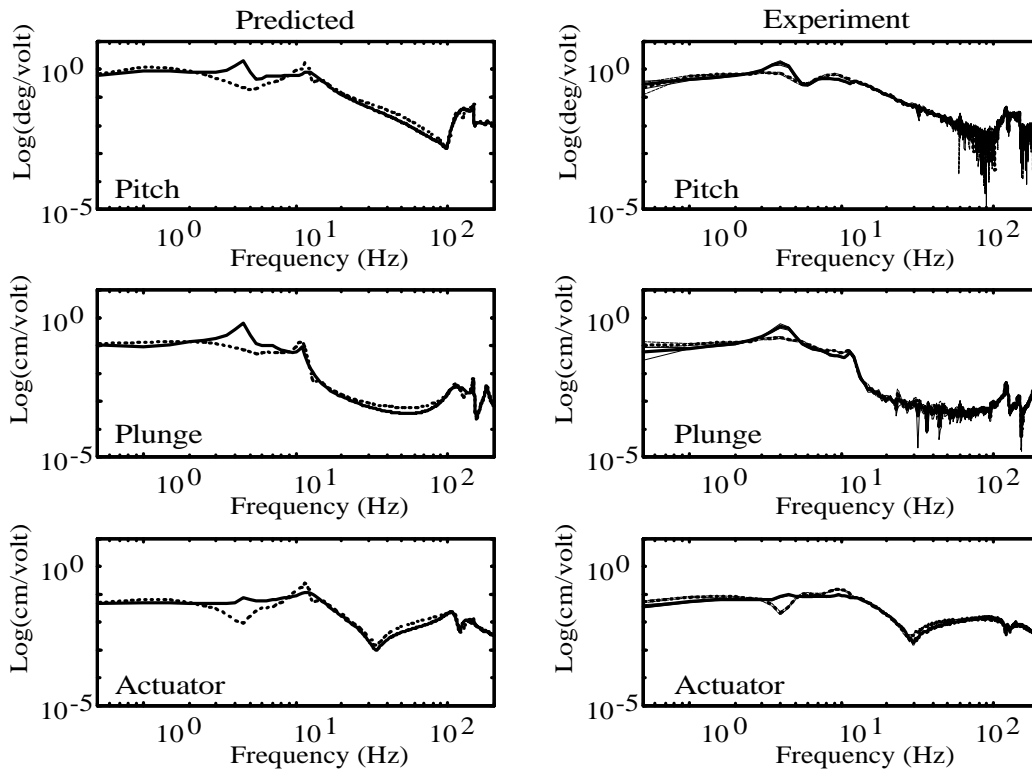
Figure 8: Analytical and Experimental FRFs at a Flow of 18.1 m/s; Open-loop (——); Closed-loop (- - -)
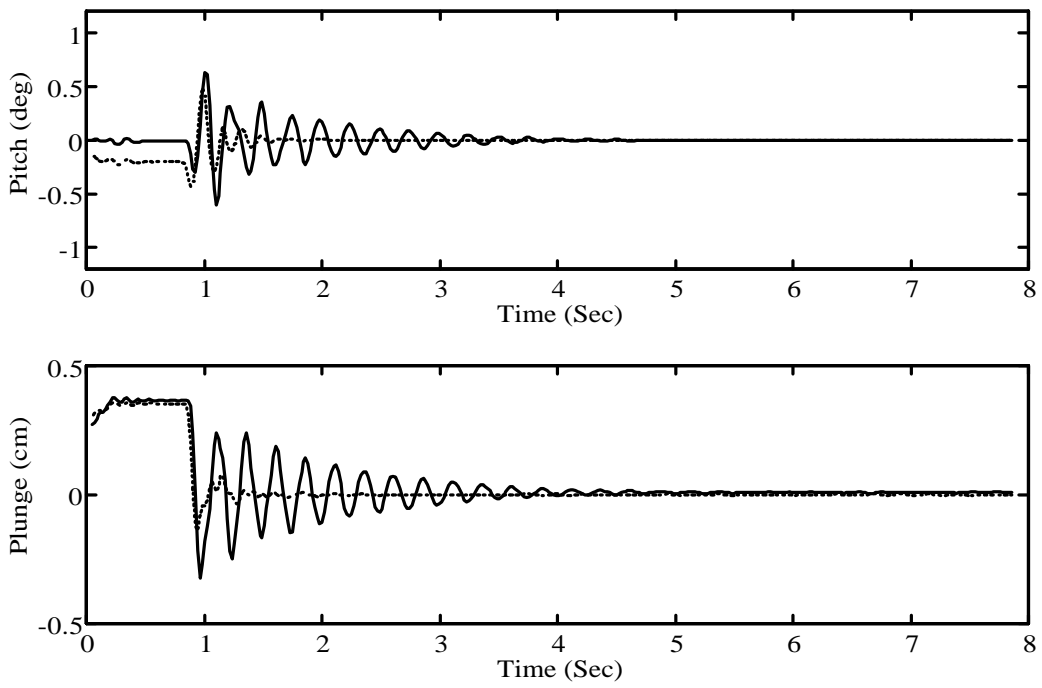
Figure 9: Transient Response With and Without Control at a Flow of 12.5 m/s; Open-loop
(| {); Closed-loop (- - -)
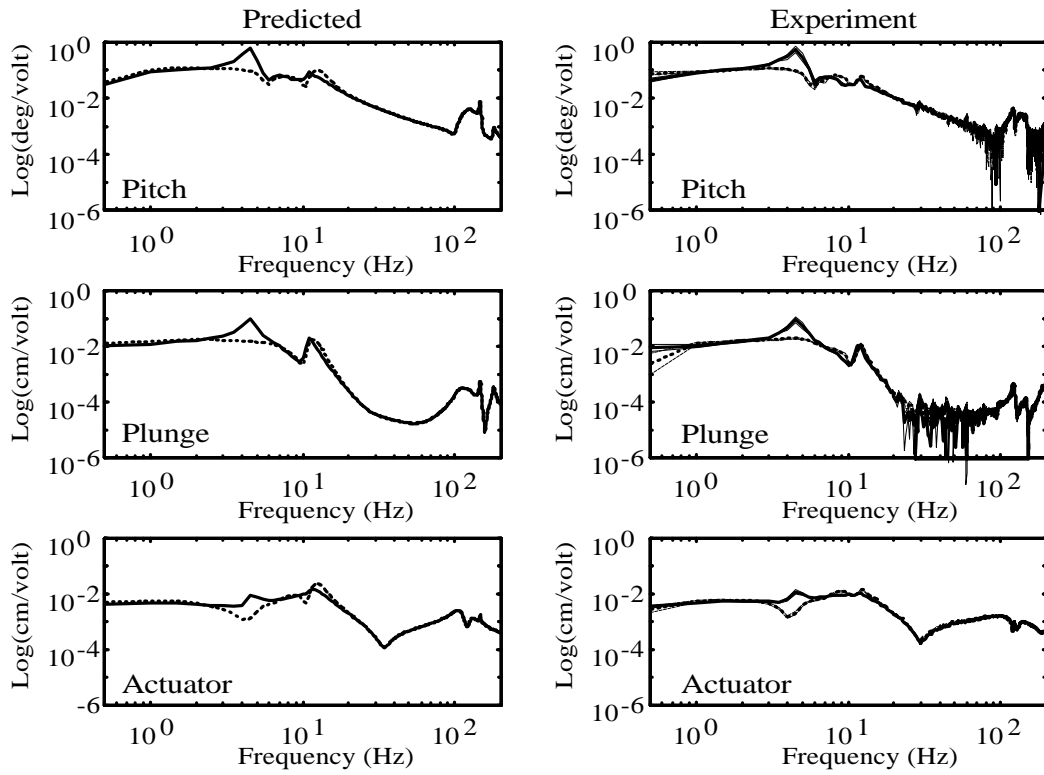
Figure 10: Open (⎯) and Closed-loop (- - -) Response at a Flow of 18.1 m/s
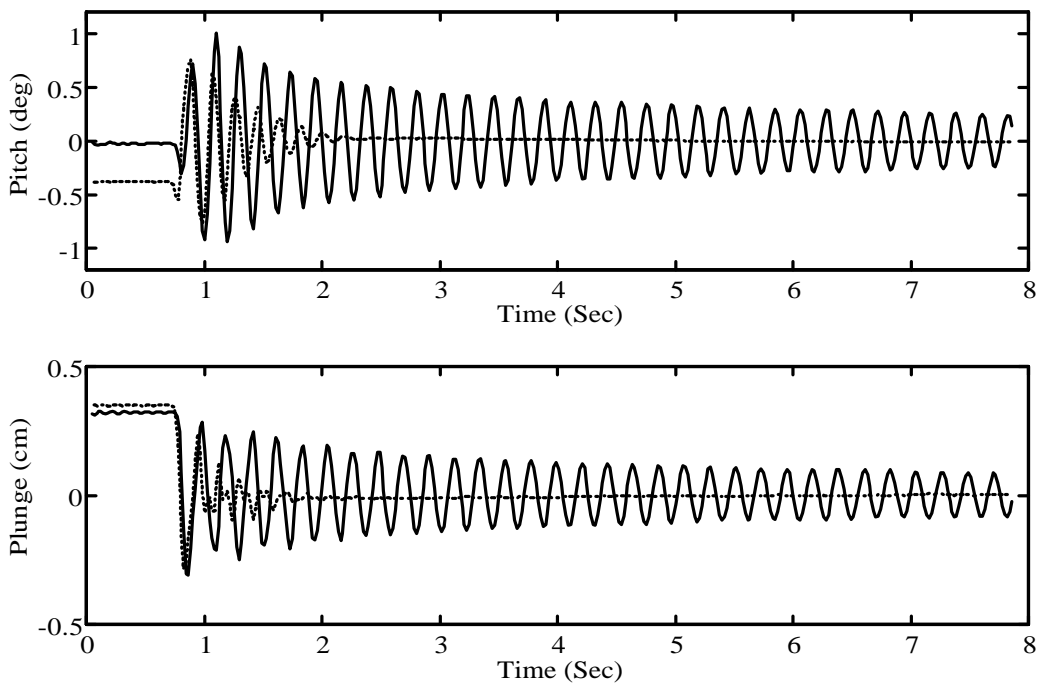
Figure 11: Transient Response With (- - -) and Without (|{) Control at a Flow of 18.1 m/s

26
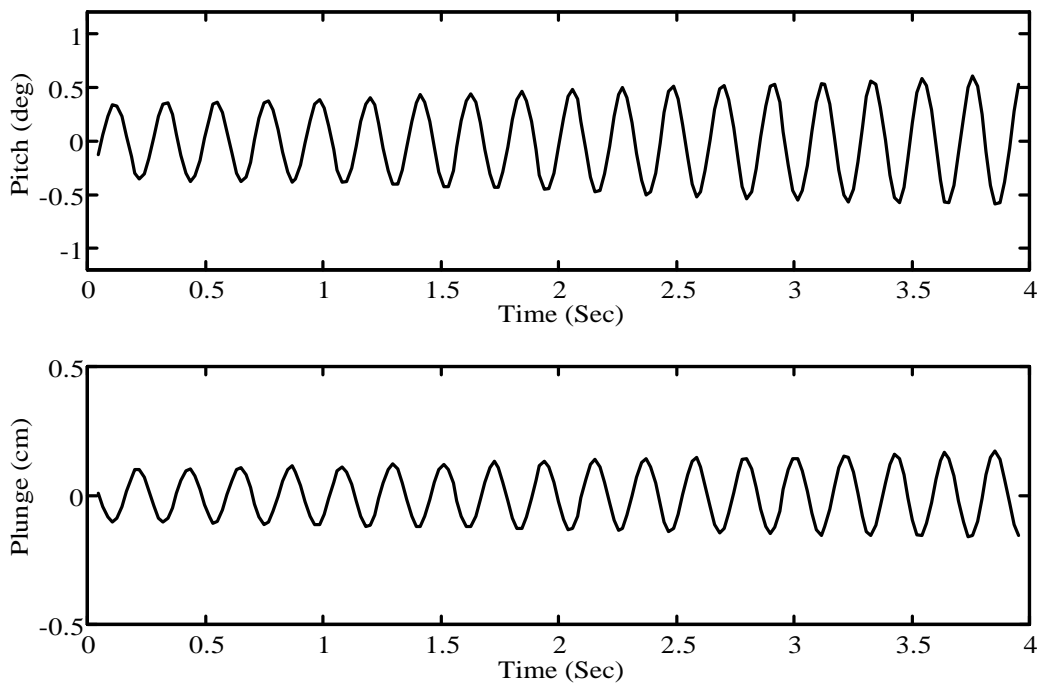
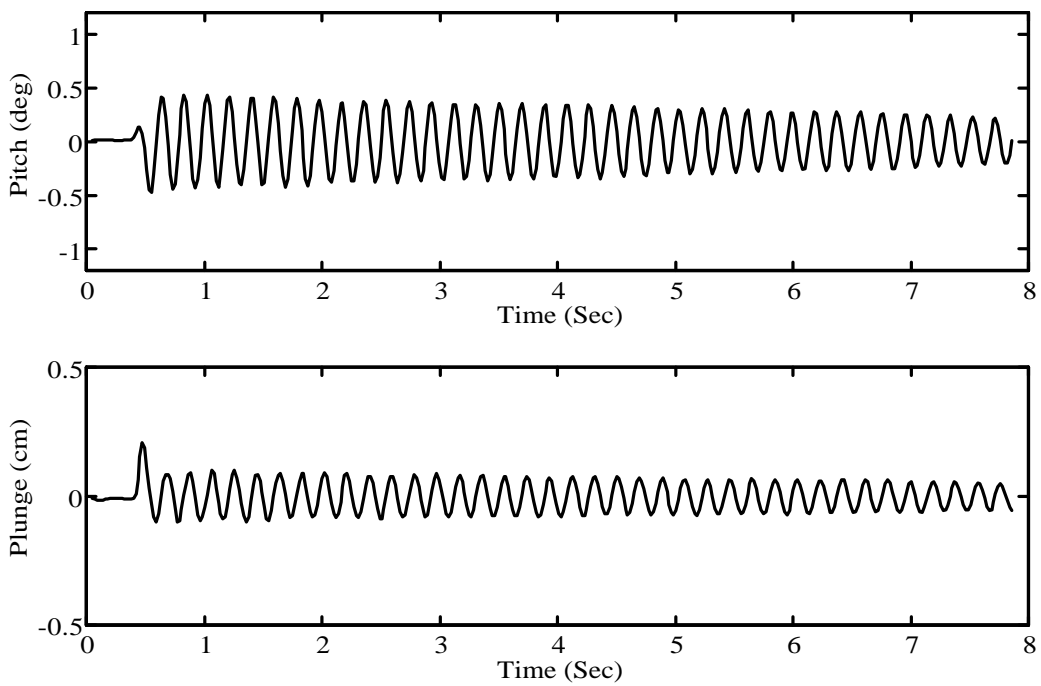Figure 12: Unstable Transient Response Without Control at a Flow of 18.6 m/s

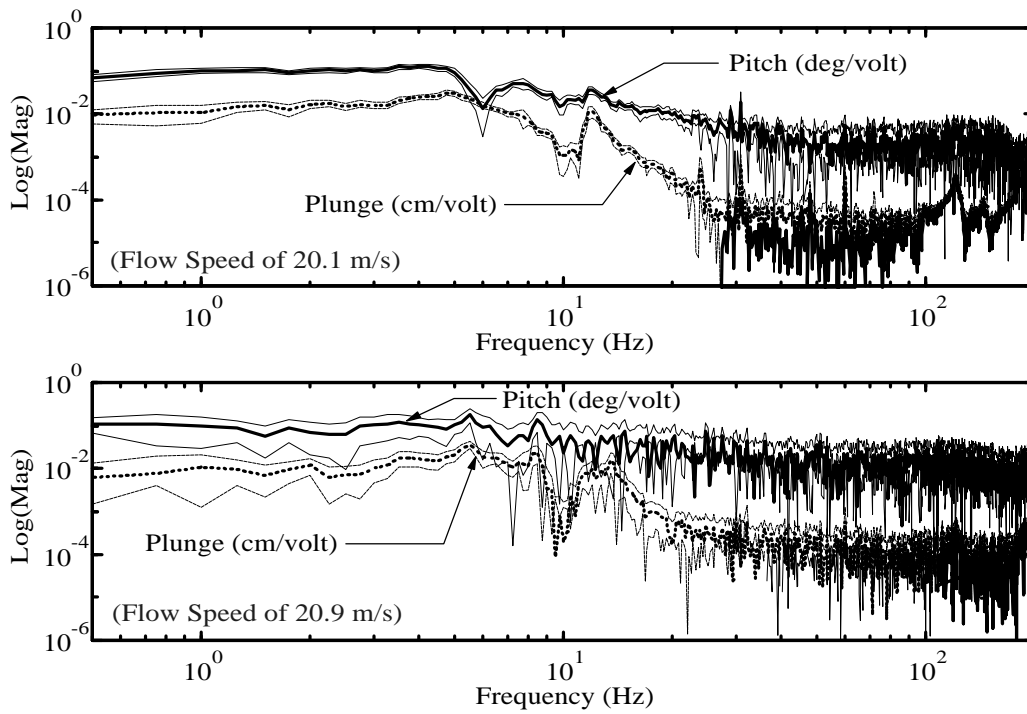Figure 13: Closed-Loop Transient Response 8.1% Above the Uncontrolled Flutter Boundary

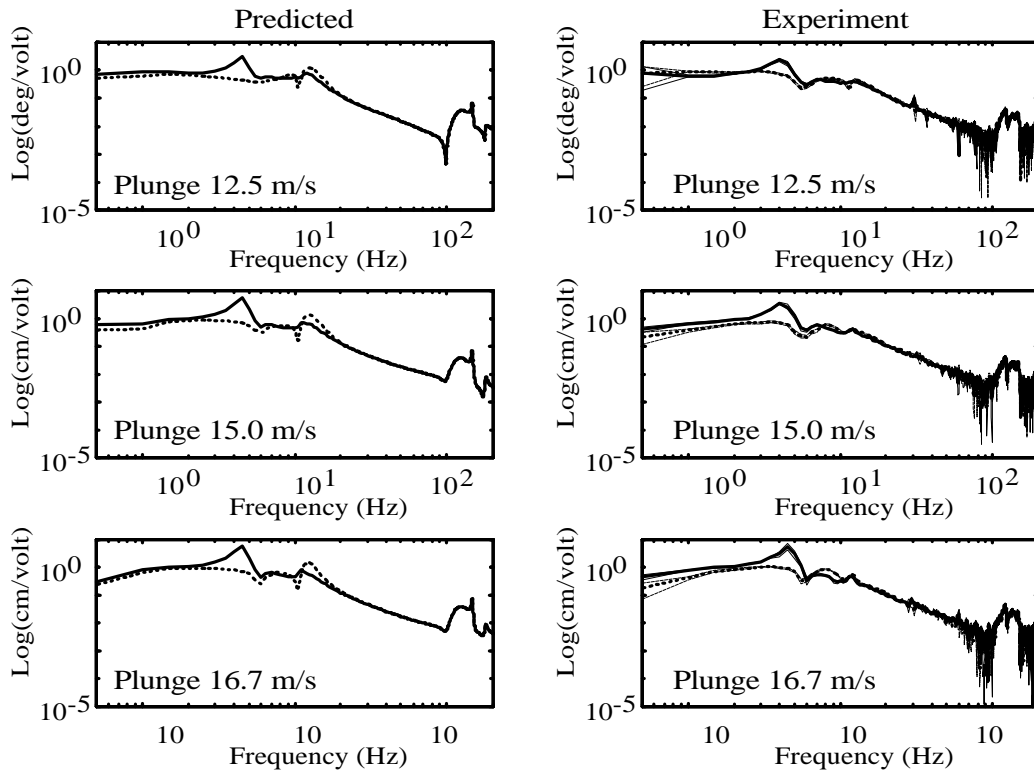Figure 14: Closed-loop Frequency Responses for 20.1 and 20.9 m/s Flowrates

Figure 15: Open (——) and Closed-loop (- - -) FRFs for O®-Nominal Flowrates